ACS OMEGA

Open Access

http://pubs.acs.org/journal/acsodf

Article

Boosting the Ionic Conductivity of Pyrrolidinium-Based Ionic Plastic Crystals by LLZO Fillers

Kotoko Ariga, Shuho Akakabe, Ryotaro Sekiguchi, Morgan L. Thomas, Yuko Takeoka, Masahiro Rikukawa, and Masahiro Yoshizawa-Fujita*

Cite This: *ACS Omega* 2024, 9, 22203−22212

Read Online

ACCESS | Metrics & More | Article Recommendations | Supporting Information

ABSTRACT: Organic ionic plastic crystals (OIPCs) have attracted attention as novel organic solid electrolyte materials, but their insufficient mechanical strength and ionic conductivity have prevented their application. In this study, a lithium salt, lithium bis(fluorosulfonyl)amide (LiFSA), and an inorganic solid electrolyte, $Li_7La_3Zr_2O_{12}$ (LLZO), were added to an OIPC, *N*,*N*-diethylpyrrolidinium bis(fluorosulfonyl)amide ([C_2epyr][FSA]). The fabricated organic−inorganic hybrid solid electrolytes were evaluated thermally, mechanically, and electrochemically to reveal which factors affect the properties of the electrolytes. All samples showed excellent thermal stability regardless of LiFSA or LLZO concentration, and they were found to be highly plastic and ion-conductive solids at a wide range of temperatures. It was also revealed that the addition of LLZO raised the nanoindentation stiffness (H_{IT}) of the [C_2epyr][FSA]/LiFSA composites. The ionic conductivity of the hybrid electrolytes was higher than that of the pristine OIPC, reaching a value of 2.1×10^{-4} S cm^{-1} at 25 °C upon addition of appropriate amounts of LiFSA and LLZO. Overall, samples with higher LiFSA concentration and moderate LLZO concentration exhibited higher ionic conductivity. Cyclic voltammetry results showed that the [C_2epyr][FSA]/LiFSA/LLZO composites were lithium-ion conductors. These findings indicate that by optimizing the concentrations of lithium salt and LLZO, it would be possible to realize their applications as solid electrolytes.

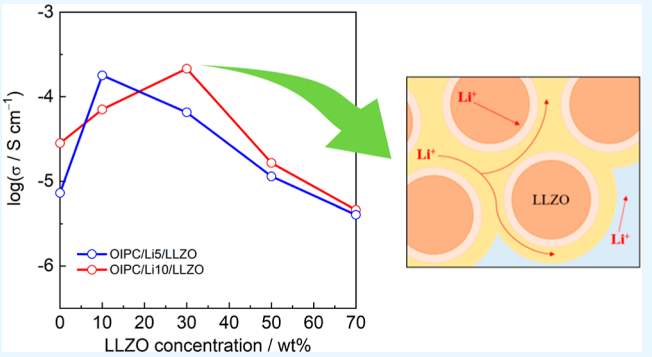

1. INTRODUCTION

Lithium-ion batteries (LIBs) are widely and effectively applicable to various devices, such as mobile phones and electric vehicles, because of their high energy density, good cycling performance, and usability over a wide range of temperatures. However, LIBs still have some safety problems due to the use of flammable liquid electrolytes which can easily leak, decompose, and cause undesirable reactions with active materials of the electrodes.[1,2] Improving the safety level of LIBs is one of the keys to a wider range of applications of LIBs in the future. All-solid-state batteries, which have no risk of electrolyte leakage, are expected to solve the safety problems of current LIBs. They also have other advantages such as higher mechanical strength, fewer side reactions between electrolytes and electrodes, a wider electrochemical window of electrolytes, and theoretically higher energy density.[3] However, the commercialization of all-solid-state batteries still faces many challenges; at this stage, they are inferior to conventional liquid-based devices with regard to both ionic conductivity and stability. This is partly due to the hard surfaces of solid electrolytes, leading to problems with the interface with electrode active materials.[4] Hence, efforts are being made to improve the conductivity and stability of all-solid-state batteries.[5]

The solid electrolyte is the essential part of all-solid-state batteries. Many kinds of inorganic and organic solid electrolytes have already been developed.[6−8] As organic electrolytes, poly(ethylene oxide) (PEO)-based solid polymer electrolytes have been well-studied. Such PEO systems have also been combined with other materials, such as poly(*m*-phenylene isophthalamide)[9] and succinonitrile,[10] to realize high ionic conductivity and mechanical strength. Also, organic electrolytes often combine inorganic electrolytes to produce solid-state electrolytes with higher performance. For example, Fang et al. developed a composite polymer electrolyte membrane incorporating a sodium beta-alumina ceramic electrolyte.[11] Various composite electrolytes obtained by combining different kinds of electrolytes are under development. Among such

Received: February 4, 2024
Revised: March 28, 2024
Accepted: April 16, 2024
Published: May 9, 2024

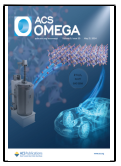

composite electrolytes, those containing organic ionic plastic crystals (OIPCs) possess several advantages. OIPCs exhibit the plastic crystal phase (PC phase), the mesophase between the solid and the liquid phases.[12] In the PC phase, molecules and ions are arranged in an ordered fashion but move in a rotational and translational manner. This is why the plasticity of OIPCs is like a liquid but with the rigid shape of a solid at room temperature. In addition to plasticity, the OIPCs of interest for battery application have many other favorable properties for safety and efficiency: low flammability, negligible volatility, and relatively high ionic conductivity for a solid. Some OIPCs are being studied as materials for solid electrolytes.[13−15] The thermal and electrochemical properties of OIPCs are very different depending on the type of cation and anion of which they are comprised.[16] Some of the previous works[17−19] have shown that *N*,*N*-diethylpyrrolidinium bis(fluorosulfonyl)amide, or [C_2epyr][FSA] (see Figure 1), has

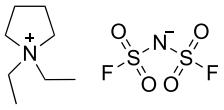

Figure 1. Chemical structure of [C_2epyr][FSA].

suitable properties for a solid electrolyte: high thermal stability (a decomposition temperature of 300 °C) and the highest ionic conductivity (9.6×10^{-6} S cm^{-1} at 25 °C) ever observed for OIPCs. The ionic conductivity of OIPCs can be enhanced by doping with small amounts of lithium salt.[20] Yamada et al. reported that [C_2epyr][FSA] doped with 5 mol % of LiFSA exhibited an ionic conductivity of 6.4×10^{-5} S cm^{-1} at 25 °C.[19] Since the level of ionic conductivity of pristine OIPCs is much lower than that of current liquid electrolytes, lithium salt doping is required for the application of the pristine OIPCs in all-solid-state batteries.

Despite the many advantages mentioned above, the level of ionic conductivity and lack of mechanical strength of the OIPCs are problems that must be overcome to enable their use in devices to replace the current batteries. To render the OIPCs more suitable as electrolytes, researchers have added various other materials to them to form novel composites. OIPCs were mixed with poly(vinylidene difluoride) (PVDF) nanofibers and PVDF nanoparticles, and their composites exhibited unique properties.[21−23] For example, Nti et al. fabricated OIPC/PVDF nanoparticle composites and found that PVDF particles reduce the degree of crystallinity of OIPCs, resulting in higher ionic conductivity [ionic conductivity of *N*-ethyl-*N*-methylpyrrolidinium bis(trifluoromethylsulfonyl)amide ([C_2mpyr][TFSA]) at 30 °C increased from 3.87×10^{-9} to 5.86×10^{-8} S cm^{-1} when 10 vol % PVDF was added].[24] Wang et al. reported that when OIPC [triethylmethylammonium bis(fluorosulfonyl)amide], LiFSA, and PEO were combined, the ionic conductivity of the composite containing 30 wt % of PEO reached 2.14×10^{-4} S cm^{-1} at 50 °C.[25] Besides polymers, ceramic nanoparticles have also been added to OIPCs in order to improve their properties. According to Adebahr et al., the addition of 10 wt % nanosized TiO_2 to [C_2mpyr][TFSA] resulted in an increase in ionic conductivity.[26] It was also reported that the addition of SiO_2 nanoparticles was effective to raise the conductivity of [C_2mpyr][TFSA].[27,28] However, when added to Li-doped [C_2mpyr][TFSA], SiO_2 resulted in composites that were less conductive, unless the particles were first functionalized with lithium propanesulfonate.[29]

$Li_7La_3Zr_2O_{12}$ (LLZO), a garnet-type inorganic electrolyte, has also been studied as a favorable additive to OIPCs. This combination of electrolytes is expected to overcome the mechanical weaknesses of OIPCs and enhance the ionic conductivity by reducing the grain boundary resistance and the interfacial resistance of LLZO. LLZO is safe and has good ionic conductivity at room temperature, but there are still some challenges to its use in all-solid-state batteries: lithium electrodeposition,[30] high area-specific resistance (ASR), and difficulties in cell assembly due to its brittleness and stiffness.[31,32] Various efforts are currently underway to overcome these issues. Gutiérrez-Pardo et al.[33] showed that, when the LLZO electrolyte was covered with thin OIPC layers on the surfaces in contact with electrodes, the total ionic conductivity reached 1.1×10^{-3} S cm^{-1}, which is the highest among the values achieved by the composites mentioned above (ionic conductivities required for commercial LIBs are in the order of 10^{-4} S cm^{-1}), and the ASR was reduced by about one-fifth (from 640 to 120 Ω cm^2). One problem with this OIPC layer/LLZO/OIPC layer electrolyte is the deterioration of the interlayer coating due to electrolyte degradation and reactivity. This problem regarding interlayers may possibly be solved by mixing OIPC and LLZO instead of layering them.

Considering its great potential as a novel solid electrolyte material, an OIPC, [C_2epyr][FSA], was combined with lithium salt, lithium bis(fluorosulfonyl)amide (LiFSA), and LLZO to develop organic−inorganic hybrid solid electrolytes (HSEs) in this research. It has already been revealed that after certain amounts of lithium salt and LLZO were added to [C_2epyr][FSA], the ionic conductivity was improved, while its sufficiently high thermal stability was maintained. However, there are still some questions to be answered, including the extent to which the addition of LLZO can improve the mechanical strength of the OIPCs. This study aims to further elucidate the effects of lithium salt and LLZO on the properties of electrolytes.

2. MATERIALS AND METHODS

2.1. Materials. 1-Ethylpyrrolidine (98%) was purchased from Tokyo Chemical Industry Co., Ltd. and purified by atmospheric distillation (fraction at 78 °C). Iodoethane (>98.0%, further purified by atmospheric distillation with the fraction collected at 72 °C), ethyl acetate (super dehydrated), dichloromethane (99.5%), silver nitrate (guaranteed reagent), and acetonitrile (guaranteed reagent) were purchased from FUJIFILM Wako Pure Chemical Corporation. LiFSA (99.0%) was purchased from Kishida Chemical Co., Ltd. LLZO (particle size: 3.3 μm) was donated by Niterra Co., Ltd.

2.2. Synthesis of *N*,*N*-Diethylpyrrolidinium Bis(fluorosulfonyl)amide ([C_2epyr][FSA]). [C_2epyr][FSA] was synthesized from *N*,*N*-diethylpyrrolidinium iodide (32.9 g, 0.129 mol) and LiFSA (24.4 g, 0.130 mol) following the previously reported procedure (yield: 29.5 g, 74%).[19]

2.3. Preparation of [C_2epyr][FSA]/LiFSA Composites. Given amounts of [C_2epyr][FSA] and LiFSA were weighed in a glovebox under an argon atmosphere. The concentrations of LiFSA were chosen as 5 and 10 mol %. Outside the glovebox, each reagent was dissolved in dichloromethane and then mixed and stirred overnight at room temperature. After being stirred, the mixture was vacuum-dried at 40 °C for 24 h. Here,

https://doi.org/10.1021/acsomega.4c01137
ACS Omega 2024, 9, 22203−22212

composites of [C_2epyr][FSA] and x mol % of LiFSA are denoted as OIPC/Lix (x = 5 or 10).

2.4. Preparation of [C_2epyr][FSA]/LiFSA/LLZO Composites. Composites of the LLZO and the OIPC/Li5 and LLZO were prepared by the following ball-milling method. OIPC/Li5 and LLZO, the sum of which was about 10% of the volume of a plastic container, were weighed in a glovebox under an argon atmosphere. The weight ratios of LLZO varied from 10, 30, 50, and 70 wt %. Zirconia beads (3 mmφ) were added to the same plastic container to fill 30% of the container's volume. The container was placed on a mini pot mill PSL-1 M (Ito Corporation) and crushed and mixed at 450 rpm for 2 h. The contents were then sieved, and the HSE composite alone was collected.

OIPC/Li10/LLZO composites were prepared by stirring. Given amounts of OIPC/Li10 and LLZO were added to a sample bottle in a glovebox under an argon atmosphere. The weight percent of LLZO varied from 10, 30, 50, and 70 wt %. The contents of the bottle were stirred for 5 min to produce the HSE composite. Here, composites of [C_2epyr][FSA], x mol % of LiFSA, and y wt % of LLZO are denoted as OIPC/Lix/LLZOy (x = 5 or 10 and y = 10, 30, 50, or 70).

2.5. Fabrication of [C_2epyr][FSA]/LiFSA/LLZO Pellets. A Teflon sheet (thickness: 500 μm; outer diameter: 13 mmφ; inner diameter: 10 mmφ) was pressed at 15 MPa for 10 s. The sample (70 mg) was placed in the inner circle of the sheet. Under evacuation with a vacuum pump, the sample was pressed at 12 MPa for 10 min and then at 25 MPa for 2 h.

2.6. Scanning Electron Microscopy. The surface morphology of the OIPC/Li/LLZO pellets was observed using a scanning electron microscope SU-8000 (Hitachi, Ltd.) with an accelerating voltage of 10 kV. The samples were fixed on the stage with carbon tape.

2.7. Thermal Properties. The sample was placed in an open-type aluminum pan and accurately weighed. Measurements were carried out at 25−500 °C using a thermogravimetric−differential thermal analysis (TG−DTA) 7200 instrument (Hitachi High-Tech Corporation). The N_2 gas flow rate was 200 mL min^{-1} and the heating rate was 10 °C min^{-1}.

The sample was placed in a sealed-type aluminum pan and accurately weighed. Measurements were carried out using a DSC7200 (Hitachi High-Tech Corporation). The N_2 gas flow rate was 40 mL min^{-1} and the heating rate was 10 °C min^{-1}.

2.8. Compression Test. Compression tests were carried out using a bioindenter, UNHT^3 Bio (Anton Paar), in the sinusoidal mode. OIPC/Li5 and OIPC/Li5/LLZO pellets were analyzed by the application of a load and microsinusoidal vibration by an indenter. Stiffness is calculated from the phase difference between the waves of the force and the indentation depth, which gives a depth profile of the indentation stiffness (H_{IT}). Measurements were conducted under the following conditions: The type of indenter was R500 μm spherical indenter. 0.1−3 mN and 0.5−10 mN of load were applied to OIPC/Li5 and OIPC/Li5/LLZO pellets, respectively. The strain rates were 0.025 s^{-1}(OIPC/Li5) and 0.05 s^{-1}(OIPC/Li5/LLZO). The sinus frequency was 10 Hz for all samples. The sinus amplitudes were 0.3 (OIPC/Li5) and 1 mN (OIPC/Li5/LLZO).

2.9. Complex Impedance Measurement. Complex impedance measurements were carried out at −60 to 100 °C using an impedance analyzer, VSP-300 (BioLogic), to measure the ionic conductivity of the samples. The temperature of the samples was controlled by placing the measurement cell in a thermostatic chamber, SU-261 (Espec Corp.). Kapton tape no.650S−P (Kenis, Ltd.) cut into a doughnut shape with an inner diameter of 8 mmφ and an outer diameter of 24 mmφ was glued onto a Pt electrode (16 mmφ). The sample was placed in the doughnut hole of the Kapton tape and placed in a cell, TYS-00DM01 (Toyo System Co., Ltd.), in a glovebox under an argon atmosphere. Resistance values were determined by graphical processing based on Nyquist plots of the measured data. Ionic conductivity was calculated by applying the resistance values to eq 1

$$\sigma = \frac{d}{RS} \tag{1}$$

where σ, d, R, and S are the ionic conductivity, interelectrode distance, resistance value, and sectional area, respectively.

The activation energy of ionic conduction was calculated from the inclination of the Arrhenius plot using eq 2

$$\log \sigma = \log A - \frac{E_a}{2.303 R_g T} \tag{2}$$

where σ, A, E_a, R_g, and T are the ionic conductivity, frequency factor, activation energy, gas constant, and temperature, respectively.

The frequency was changed from 100 mHz to 1 MHz. The applied voltage was 100 mV. Pt electrodes were used as the working electrode and counter electrode.

2.10. Cyclic Voltammetry. Cyclic voltammetry (CV) measurements were carried out to investigate the redox reaction of Li in the electrolytes. Kapton tape no. 650S-P (Kenis, Ltd.) cut into a doughnut shape with an inner diameter of 8 mmφ and an outer diameter of 24 mmφ was glued onto a Li electrode (16 mmφ) in a glovebox under an argon atmosphere. The sample was placed in the hole of the Kapton tape and placed in cell TYS-00DM01 (Toyo System Co., Ltd.). Measurements were carried out at 60 °C using an impedance analyzer, VSP-300 (BioLogic), in a thermostatic chamber, TB-1 (BAS Inc.), after stabilizing the cell at room temperature for 24 h. The voltage range of measurements was −0.25 to 1.0 V and the scan rate was 5.0 mV s^{-1}. The working electrode was a Ni electrode. Li electrodes were used as the reference and counter electrode.

3. RESULTS AND DISCUSSION

As mentioned above, previous studies have reported that [C_2epyr][FSA] exhibits ionic conductivity higher than that of other pyrrolidinium salts, and [C_2epyr][FSA] was used in this study to develop solid electrolytes combining OIPC and LLZO for LIBs. Scanning electron microscopy (SEM) observations were made to confirm the complexation of the complexes of the OIPC and LLZO. As a representative sample, the OIPC/Li5/LLZO70 observations are shown in Figure S1. The SEM images of OIPC/Li5/LLZO70 clearly showed that OIPC/Li5 is well-mixed with the LLZO matrix. It was found that there were no gaps between the OIPC and LLZO particles and that they were filled. Similar observations were made for the other composites.

3.1. Thermal Stability. TG−DTA measurements were carried out to evaluate the thermal stability of the [C_2epyr][FSA] and the OIPC/Lix composites. The TG curves of the samples are shown in Figure S2. The 5% weight loss temperature of the OIPC ([C_2epyr][FSA]), OIPC/Li5, and OIPC/Li10 was 295, 292, and 301 °C, respectively. These

https://doi.org/10.1021/acsomega.4c01137
ACS Omega 2024, 9, 22203−22212

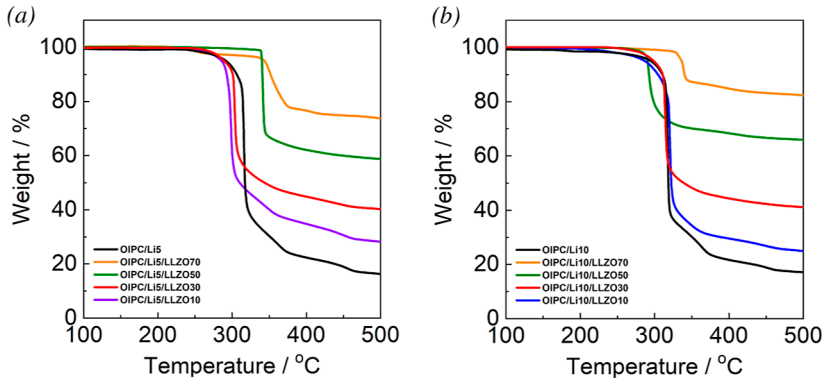

Figure 2. TG curves of the (a) crystalline OIPC/Li5/LLZO and (b) crystalline OIPC/Li10/LLZO composites.

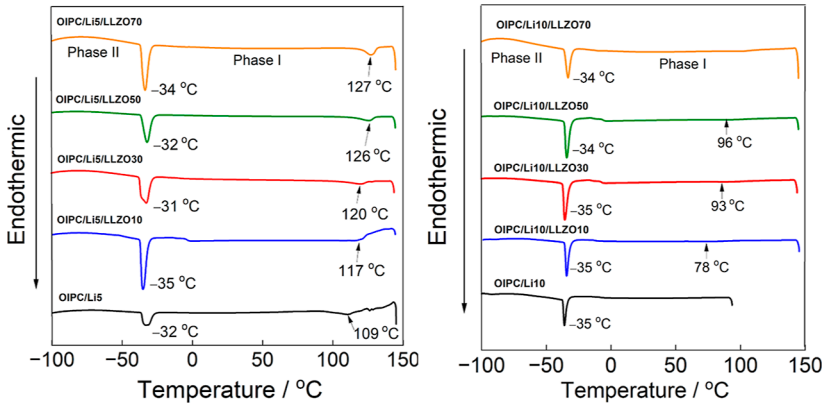

Figure 3. DSC curves of the (a) OIPC/Li5/LLZO and (b) OIPC/Li10/LLZO composites.

results indicate that the addition of lithium salt does not affect the thermal stability of the OIPC. The thermal degradation is considered to be caused by the cleavage of S−F bonds.[34,35] Considering that the minimum thermal stability requirement for LIBs is 150 °C, all of these [C_2epyr][FSA] and OIPC/Li*x* composites have sufficient thermal stability as electrolytes.

TG curves of the OIPC/Li5 and OIPC/Li5/LLZO composites are shown in Figure 2a and those of the OIPC/Li10 and OIPC/Li10/LLZO are shown in Figure 2b. For the OIPC/Li5/LLZO composites, the LLZO content of each sample, which was calculated from the residual mass of OIPC/Li5, LLZO, and the corresponding OIPC/Li5/LLZO composite at 500 °C, was almost the same as its planned LLZO ratio. The 5% weight loss temperatures of OIPC/Li5, OIPC/Li5/LLZO10, 30, 50, and 70 were 292, 286, 289, 316, and 343 °C, respectively. Although the samples with 30 wt % or less LLZO showed no improvement in thermal stability, the composites became more thermally stable as the amount of LLZO added increased. Thus, the addition of LLZO can improve the thermal stability of OIPC/Li. The 5% weight loss temperatures of OIPC/Li10, OIPC/Li10/LLZO10, 30, 50, and 70 were 295, 287, 299, 290, and 345 °C, respectively. The thermal stability was almost the same for the composites with 0−50 wt % of LLZO concentration, but it increased by about 50 °C when 70 wt % of LLZO was added. The weight loss is mostly attributed to the degradation of OIPC/Li because the residual mass of pure LLZO at 500 °C is reported to be 97.2%.[32] S−F bonds, whose cleavage is the leading cause of the thermal degradation,[34,35] are present in [C_2epyr][FSA] and LiFSA but not in LLZO, so we can expect that the temperature where OIPC/Li/LLZO composites begin to lose weight becomes higher as the LLZO content increases. The somewhat different profile of the TGA curve for 50 wt % LLZO is thought to be due to the ratio of OIPC/Li to LLZO. In OIPC/Li10/LLZO50, the disordered interphase of OIPC/Li formed at the surface of LLZO particles is considered to be larger than that in OIPC/Li10/LLZO10 and 30 (regardless of whether it is connected or isolated). This may make the cleavage of the S−F bonds more facile. In the same way, the disordered interphase of OIPC/Li10/LLZO70 may be larger than that of LLZO50. However, it contains more LLZO than does the case for OIPC/Li, and thus, the excess amount of LLZO would have a greater impact upon the thermal stability in the case of the OIPC/Li10/LLZO70. All of the composites had sufficient thermal stability as an electrolyte for LIBs despite the differences depending on the LLZO concentration.

3.2. Phase-Transition Behavior. Differential scanning calorimetry (DSC) measurements were carried out to evaluate the phase-transition behavior of the [C_2epyr][FSA] and the OIPC/Li*x* composites. DSC curves (second heating scan) of the samples are shown in Figure S3. The solid phases were designated as phase I and phase II in the order of higher temperature. The temperature range of measurement was −150 to 150 °C except for that of OIPC/Li10, which showed no clear melting point. The solid−solid phase-transition temperatures of [C_2epyr][FSA], OIPC/Li5, and OIPC/Li10 were −34, −32, and −35 °C, respectively, indicating that the addition of lithium salt has no effect on the solid−solid phase transition of the OIPC. On the other hand, the melting point decreased from 131 to 109 °C when 5 mol % of LiFSA was added. Such a decrease is a typical characteristic of the Li-doped plastic crystal systems.[19,22,36] It should be the result of

https://doi.org/10.1021/acsomega.4c01137
ACS Omega 2024, 9, 22203−22212

disorder within the system caused by eutectic reactions between the OIPC and the lithium salt. OIPC/Li10 showed no clear melting point. This disappearance of melting points suggests that the system was further disordered by the addition of a larger amount of lithium salt. For OIPC/Li10, the DSC measurement was carried out only up to 100 °C. It was already reported that the OIPC/Li10 sample exhibited no melting point above 100 °C.[37]

DSC curves (second heating scan) of the emulsion of OIPC/Li5/LLZO are shown in Figure 3a and those of the emulsion of OIPC/Li10/LLZO are shown in Figure 3b. The solid−solid phase-transition temperatures were around −34 °C for all samples regardless of the amount of lithium salt or LLZO added. As for OIPC/Li5/LLZO composites, the melting points increased and the temperature range of phase I expanded as the amount of LLZO increased. This means that LLZO extends the operating temperature range of the OIPC/Li*x* composites as solid electrolytes. The melting points of OIPC/Li10/LLZO composites showed almost the same tendency, while no clear melting point was observed in the samples containing 0 and 70 wt % of LLZO. At the same LLZO concentration, the OIPC/Li10 samples exhibited a lower and broader melting point than the analogous OIPC/Li5 samples, indicating that the former was more disordered than the latter. This can be attributed to the increase of the liquid phase and well-coated LLZO particles in the system.

3.3. Mechanical Strength. Compression tests were carried out to evaluate the mechanical strength of OIPC/Li5 and the OIPC/Li5/LLZO pellets. Figure 4 shows the

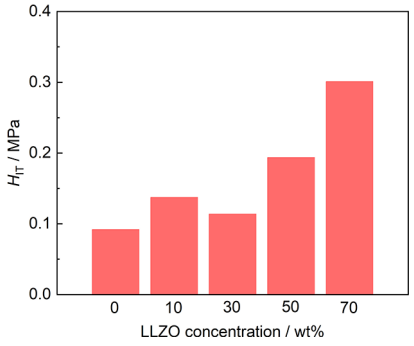

Figure 4. H_{IT} of OIPC/Li5 and OIPC/Li5/LLZO composites.

nanoindentation stiffness (H_{IT}) of the samples. The H_{IT} of OIPC/Li5 was 0.0920 MPa. It is likely that this low value is due to eutectic reactions between [C_2epyr][FSA] and LiFSA. The H_{IT} increased with increasing LLZO concentration, and the H_{IT} of OIPC/Li5/LLZO70 (0.30 MPa) was about 3 times higher than that of pure OIPC/Li5 without LLZO. The slight decline observed with OIPC/Li5/LLZO30 is possibly caused by the formation of the disordered OIPC/Li layer between OIPC/Li and LLZO, which will be discussed in a later section. The contact area of the OIPC/Li and LLZO, where this disordered layer is formed, will increase as the LLZO content increases. This is probably why the H_{IT} of the LLZO30 sample was lower than that of LLZO10. However, when LLZO content becomes higher, the mechanical strength of the composite electrolytes will be more dependent on the stiffness of LLZO. For these reasons, the H_{IT} of the OIPC/Li/LLZO composites reached the highest value with an intermediate amount of LLZO. The H_{IT} increased again with more LLZO, indicating that the disordered layer got thinner, and the stiffness of LLZO became more responsible for the whole mechanical strength. From these results, it is concluded that [C_2epyr][FSA]/LiFSA can be mechanically strengthened by the addition of LLZO, while the H_{IT} of pure LLZO should be measured to reveal the mechanism behind this mechanical improvement.

In the case of 18650 format LIBs, the most widely used type of LIBs,[38] the internal pressure buildup of the cells is less than 2.5 MPa even when the cells are heated at a rate of 4.8 °C min^{-1} to reach 150 °C at the surface.[39] It suggests that the stiffness obtained from the OIPC/Li/LLZO samples still require improvement to be used in real batteries. However, these results gave us an important insight that we can adjust the stiffness of solid-state electrolytes by changing the ratio of mixed ceramic particles. In considering the applications, some questions should also be answered; whether the internal pressure of all-solid-state LIBs changes in the same manner as the current LIBs, how stable the electrolyte can be when it is exposed to external shocks other than thermal abuse, etc. These points of view will be considered in future studies.

3.4. Ionic Conductivity. Complex impedance measurements were carried out to evaluate the ionic conductivity of the [C_2epyr][FSA] and the OIPC/Li*x* composites. Arrhenius plots of ionic conductivities for the samples are shown in Figure S4. The plots were linear and showed an Arrhenius-type temperature dependence,[40] i.e., these electrolytes have hopping conduction of ions.[41] In all samples, the ionic conductivity rose sharply at around −30 to −40 °C. This temperature range is almost identical to the solid−solid phase-transition temperatures (from phase II to phase I) observed by DSC measurements. It is thought that the presence of phase I, the most plastic and therefore conductive solid phase, made the ions highly mobile and thus increased the ionic conductivity. The activation energy of ionic conduction was calculated from the slope of the Arrhenius plots using eq 2 and is presented in Table S1. The activation energy of ionic conduction of [C_2epyr][FSA], OIPC/Li5, and OIPC/Li10 was almost the same: 27.9, 30.5, and 24.7 kJ mol^{-1}, respectively. It means that the mechanism of ionic conduction does not change depending on the lithium-salt concentration. Table S1 also shows the ionic conductivity at 25 °C. The ionic conductivity of [C_2epyr][FSA], OIPC/Li5, and OIPC/Li10 was 2.4×10^{-6}, 7.3×10^{-6}, and 2.8×10^{-5} S cm^{-1} at 25 °C, respectively. The ionic conductivity was improved as the lithium-salt concentration increased. This implies that the accumulation of liquid phases distributed in the matrix of OIPC/Li composites occurred as the amount of lithium salt increased, and when the amount of lithium salt reaches at a certain level, they form new interconnected liquid pathways where ions can be transported, as suggested by Henderson et al.[42]

Arrhenius plots of the corresponding OIPC/Li5/LLZO are shown in Figure 5a and those of the corresponding OIPC/Li10/LLZO are shown in Figure 5b. The plots were linear and showed an Arrhenius-type temperature dependence, as was observed for [C_2epyr][FSA] and the OIPC/Li*x* composites. The activation energy of ionic conduction was calculated from the slope of the Arrhenius plots and is presented in Table S1. Although there are some minor exceptions, the activation energy slightly increased as the LLZO concentration increased. This may be because the presence of LLZO prevents ion hopping within the defects, and the bulk of LLZO becomes the main conduction path. However, the addition of LLZO did not drastically change the mechanism of ionic conduction. In all

https://doi.org/10.1021/acsomega.4c01137
ACS Omega 2024, 9, 22203−22212

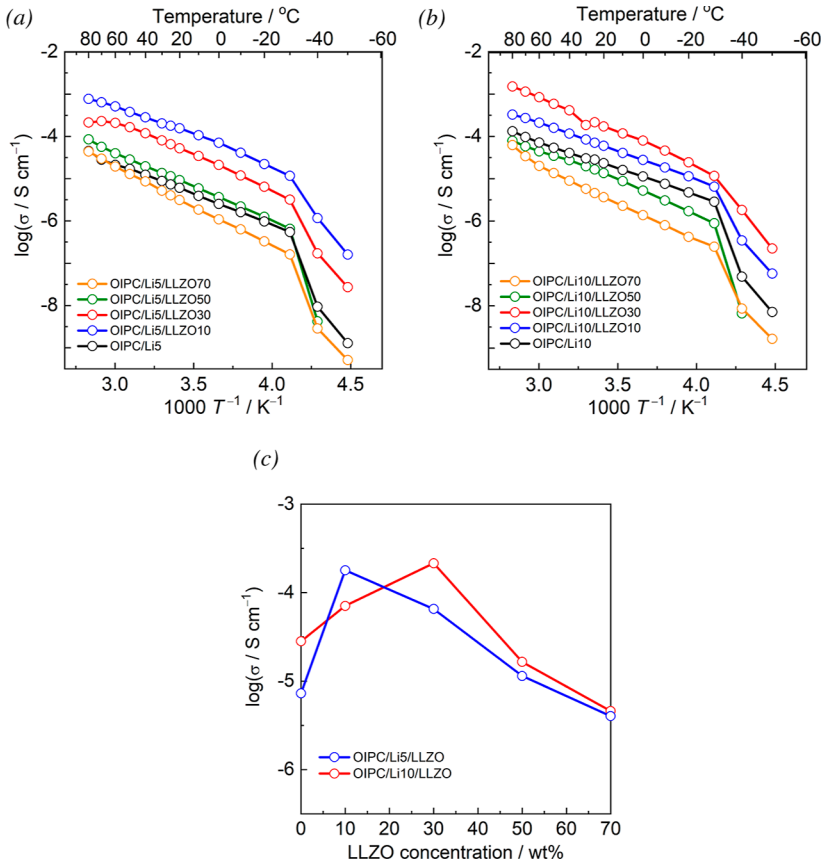

Figure 5. Arrhenius plots of ionic conductivities for (a) OIPC/Li5 and OIPC/Li5/LLZO composites and (b) OIPC/Li10 and OIPC/Li10/LLZO composites and (c) LLZO concentration dependence of ionic conductivity at 25 °C for OIPC/Li*x*/LLZO*y*.

the samples, the ionic conductivity increased sharply at around −30 to −40 °C.

This temperature range is almost identical to the solid−solid phase-transition temperatures observed by the DSC measurements. As in the case of the OIPC/Li composites, this jump in ionic conductivity is considered to be attributed to phase I. Regardless of the LLZO concentration, the ionic conductivity became higher as the temperature increased.

Figure 5c describes the relationships between LLZO concentration and ionic conductivity of the OIPC/Li5/LLZO and the OIPC/Li10/LLZO at 25 °C. The ionic conductivity of the OIPC/Li5/LLZO10 was 1.8×10^{-4} S cm^{-1} at 25 °C, which was about 25 times higher than that of the OIPC/Li5. Further addition of LLZO decreased the ionic conductivity. The ionic conductivity at 25 °C reached the highest value of all, 2.1×10^{-4} S cm^{-1}, when 30 wt % of LLZO was added to OIPC/Li10. However, composites with higher LLZO concentration were even less conductive than the composite without LLZO. This means that there is an optimum LLZO concentration to improve the ionic conductivity, and the value is different depending on the LiFSA concentration. OIPC/Li5 and OIPC/Li10 were visually different in fluidity. It is conceivable that such differences in physical properties changed the thickness of the disordered layer and, as a result, the optimum LLZO concentration. To be more specific, more fluid OIPC/Li10/LLZO composites required a larger amount of LLZO than the amount of the OIPC/Li5/LLZO samples to form a stable interphase between the OIPC/Li and LLZO.

In the present study, composites were prepared by mixing OIPC and unsintered LLZO. The process of sintering is costly, and both energy and time intensive (e.g., at 1200 °C for 36 h),[43] so we did not do that process in this study. LLZO is a solid electrolyte and has a good ionic conductivity at room temperature, as already mentioned. However, the ionic conductivity of unsintered LLZO is low due to a high grain boundary resistance. Pellets of unsintered LLZO were prepared, and their ionic conductivity was measured. The results showed that the ionic conductivity of the unsintered LLZO was below 10^{-9} S cm^{-1} at room temperature (Figure S5). After the addition of LLZO to the OIPC/Li, the ionic conductivity of the OIPC/Li increased. It is considered that the increased ionic conductivity of the OIPC/Li composite is not a result of the contribution from the ionic conduction of LLZO but rather the influence of the LLZO surface.

It is suggested that the formation of a disordered interphase of the OIPC/Li on LLZO particles increases the ionic conductivity. Nti et al.[44] reported similar tendencies for *N*-ethyl-*N*-methylpyrrolidinium bis(fluorosulfonyl)amide ([C_2mpyr][FSA])/PVDF composite electrolytes, suggesting that a PVDF-rich interphase and disordered OIPC interphase were formed between [C_2mpyr][FSA] and PVDF. The formation of the disordered interphase of [C_2mpyr][FSA] was supported by DSC results and ^{1}H NMR spectra. Nti et al.[44] also reported that the results of Fourier-transform infrared (FTIR) spectroscopy showed that new hydrogen bonds were formed between [C_2mpyr][FSA] and PVDF and such a strong interaction could create the disordered interphase. [C_2mpyr]-[FSA]/PVDF exhibited the highest conductivity when the

https://doi.org/10.1021/acsomega.4c01137
ACS Omega 2024, 9, 22203−22212

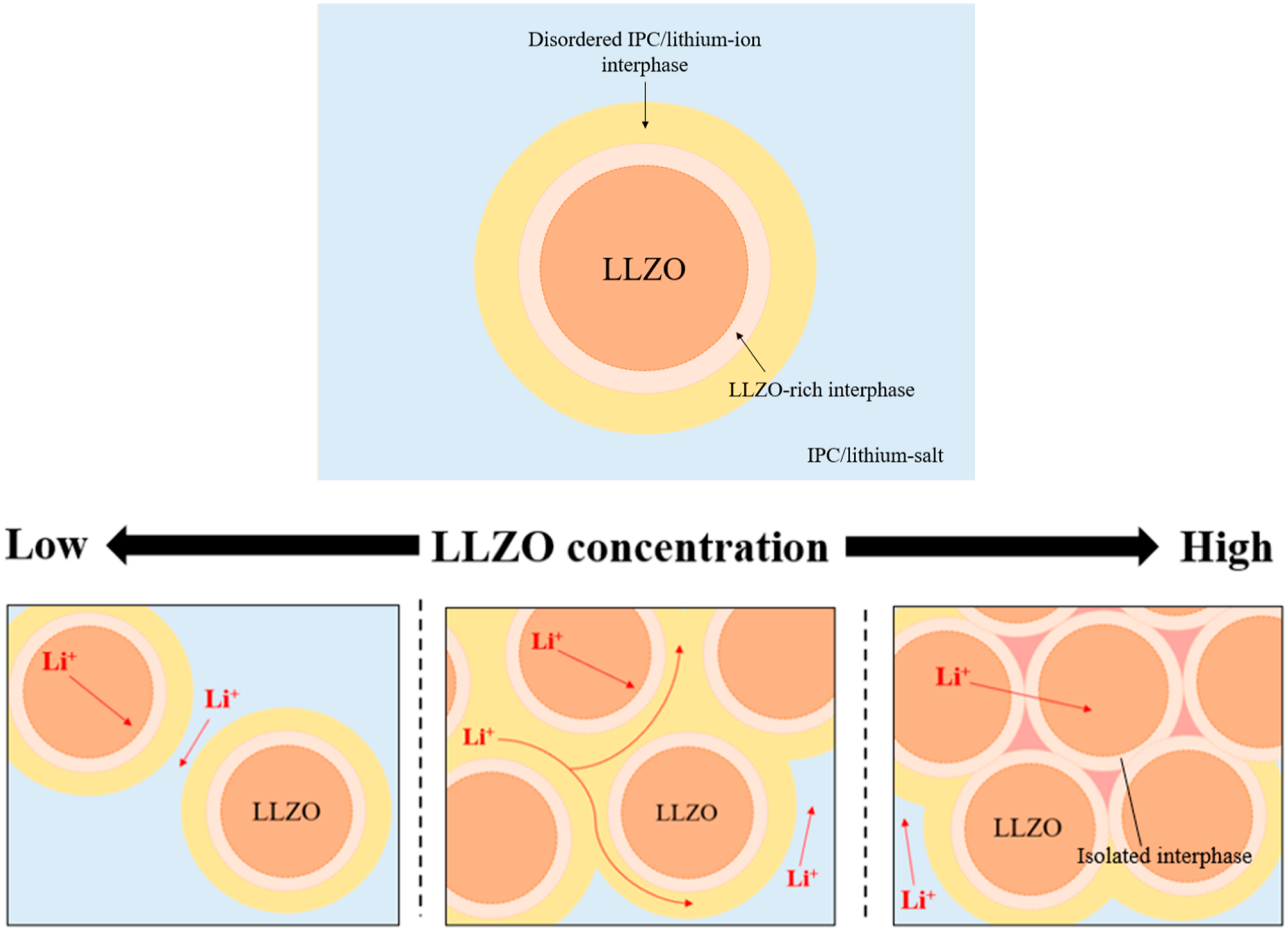

Figure 6. Schematic diagram of the proposed formation of new ion-conductive pathways at the interface between the ion-conducting ligands of the OIPC/Li and LLZO.

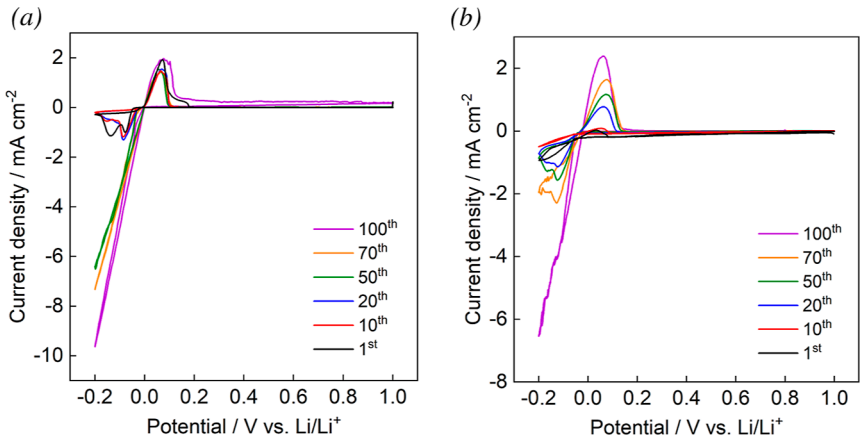

Figure 7. Cyclic voltammograms of (a) OIPC/Li5/LLZO10 and (b) OIPC/Li10/LLZO30.

PVDF concentration was 50 vol %. The additive concentration vs ionic conductivity of [C_2mpyr][FSA]/PVDF is thought to be a parallel phenomenon to that of [C_2epyr][FSA]/LiFSA/LLZO, and thus we speculate that there is a disordered [C_2epyr][FSA]/LiFSA interphase. In the systems with a disordered interphase, the ionic conductivity increases as the amount of additives increases because the distance between the particles decreases and the interphase gradually interconnects (Figure 6).[44] However, when the percolation threshold is exceeded, the additive particles begin to overlap, and the disordered interphase becomes isolated (Figure 6) and the volume of less conductive (e.g., nonsintered LLZO and PVDF) materials increases. This is the cause of the "highest in the middle concentration" tendency of ionic conductivity seen in OIPC/Li10/LLZO. The initial increase can also be attributed to the formation of a space charge layer, a region where positive or negative charges accumulate locally, at the interface between [C_2epyr][FSA]/LiFSA and LLZO.[29,45,46] Further investigation, including ^{1}H NMR and FTIR, is required to support these hypotheses.

https://doi.org/10.1021/acsomega.4c01137
ACS Omega 2024, 9, 22203−22212

3.5. Redox Behavior of Li. CV was carried out to evaluate the cyclic performance of the electrolytes. As for OIPC/Li5 and OIPC/Li10, peaks derived from oxidation of Li were observed at around 0.1 V vs Li/Li^+ and those derived from reduction of Li were observed at −0.2 V vs Li/Li^+ in all cycles from first to 100th (Figure S6). This demonstrates that these [C_2epyr][FSA]/LiFSA composites conduct lithium ions. A broad reduction behavior was observed in each cycle for the phosphorus of OIPC/Li5. OIPC/Li10 also showed two reduction peaks when the number of cycles was low. These may have been caused by the overpotential required for some of the lithium ions to be reduced.

The cyclic performance of the OIPC/Li/LLZO composites with high ionic conductivity was also examined. Figure 7a,b shows cyclic voltammograms of OIPC/Li5/LLZO10 and OIPC/Li10/LLZO30, respectively. As with the OIPC/Li composites, both exhibited peaks derived from oxidation and reduction of Li in all cycles from first to 100th, meaning that the OIPC/Li/LLZO composites can also work as lithium-ion conductors. Oxidation peaks were observed at about 0 V vs Li/Li^+ and reduction peaks were observed at around −0.2 to −0.1 V vs Li/Li^+. There were one oxidation peak and two reduction peaks in each cycle when the cycle number was low, but a single reduction peak appeared when the cycle number reached a certain figure. The two reduction peaks may be attributed to the presence of an overpotential. Compared with OIPC/Li composites (Figure S6), the current density of both oxidation and reduction became larger after LLZO was added. It means that LLZO has the effect of improving the oxidation and reduction of Li. This improvement can be derived from the promoted diffusion of lithium ions caused by the disordered interphase between [C_2epyr][FSA]/LiFSA and LLZO. The diffusion coefficient is a key parameter in determining the electrochemical characteristics of a battery model.[47] Furthermore, the current density of OIPC/Li10/LLZO30 increased with further cycling, which is consistent with what was reported by Yamada et al.[19] This may be due to the change in the electrode/electrolyte interface or the localization of Li^+ through repeated voltage application.[48−50]

4. CONCLUSIONS

In this study, organic−inorganic HSEs, [C_2epyr][FSA]/LiFSA/LLZO, were prepared, and their thermal, mechanical, and electrochemical properties were studied to reveal what effects lithium salt and LLZO have on the OIPC. Each sample showed a high level of thermal stability for a solid electrolyte regardless of lithium-salt or LLZO concentrations. While the addition of LLZO had little effect on the phase-transition behavior, it expanded the temperature range of phase I with the melting point being higher. As the LLZO concentration increased, the H_{IT} values of the composites became higher, implying that LLZO enhanced the mechanical strength of the composite electrolytes. Higher LiFSA concentration resulted in higher ionic conductivity. As for OIPC/Li5/LLZO and OIPC/Li10/LLZO, the ionic conductivity reached the maximum value when 10 and 30 wt % of LLZO were added, respectively. We speculate that disordered domains of [C_2epyr][FSA]/LiFSA are formed at the interface of LLZO and that when an adequate amount of LLZO is added, they interconnect to form new ion-conducting pathways. However, further addition of LLZO decreased the ionic conductivity, suggesting that optimization of the combination of LiFSA and LLZO concentrations is required to achieve high ionic conductivity. Among all the tested samples, OIPC/Li10/LLZO30 exhibited the highest ionic conductivity of 2.1×10^{-4} S cm^{-1} at 25 °C. CV was performed with the OIPC/Li/LLZO composites which showed high ionic conductivity. The results indicated that both [C_2epyr][FSA]/LiFSA and [C_2epyr][FSA]/LiFSA/LLZO composites are lithium-ion conductors and that addition of LLZO can promote oxidation and reduction of Li in the composites. Considering all of these results, [C_2epyr][FSA]/LiFSA/LLZO composites are highly promising as an organic−inorganic HSE. Future research will be continued to reveal what interactions are taking place between OIPC/Li and LLZO and how they affect the ionic conductivity and other properties of the hybrid electrolytes in more detail.

■ ASSOCIATED CONTENT

Supporting Information

The Supporting Information is available free of charge at https://pubs.acs.org/doi/10.1021/acsomega.4c01137.

SEM images of OIPC/Li10/LLZO70; TG curves, DSC charts, Arrhenius plots of ionic conductivities, and activation energies of ionic conductivities for OIPC and OIPC/Li*x*; ionic conductivity of unsintered LLZO; and cyclic voltammograms of OIPC/Li*x* (PDF)

■ AUTHOR INFORMATION

Corresponding Author

Masahiro Yoshizawa-Fujita − *Department of Materials and Life Sciences, Sophia University, Chiyoda-ku, Tokyo 102-8554, Japan*; orcid.org/0000-0002-8269-985X; Email: masahi-f@sophia.ac.jp

Authors

Kotoko Ariga − *Department of Materials and Life Sciences, Sophia University, Chiyoda-ku, Tokyo 102-8554, Japan*

Shuho Akakabe − *Department of Materials and Life Sciences, Sophia University, Chiyoda-ku, Tokyo 102-8554, Japan*

Ryotaro Sekiguchi − *Department of Materials and Life Sciences, Sophia University, Chiyoda-ku, Tokyo 102-8554, Japan*

Morgan L. Thomas − *Department of Materials and Life Sciences, Sophia University, Chiyoda-ku, Tokyo 102-8554, Japan*; orcid.org/0000-0002-8323-3832

Yuko Takeoka − *Department of Materials and Life Sciences, Sophia University, Chiyoda-ku, Tokyo 102-8554, Japan*; orcid.org/0000-0003-4958-3879

Masahiro Rikukawa − *Department of Materials and Life Sciences, Sophia University, Chiyoda-ku, Tokyo 102-8554, Japan*

Complete contact information is available at: https://pubs.acs.org/10.1021/acsomega.4c01137

Author Contributions

The manuscript was written through contributions of all authors. All authors have given approval to the final version of the manuscript.

Notes

The authors declare no competing financial interest.

■ ACKNOWLEDGMENTS

This work was supported by a Sophia University Special Grant for Academic Research. The authors appreciate the kind

support of Fumio Morigaki and Naoya Tashiro (Anton Paar) for the rheological measurements.

REFERENCES

(1) Tarascon, J. M.; Armand, M. Issues and challenges facing rechargeable lithium batteries. *Nature* **2001**, *414* (6861), 359−367.
(2) Chen, Y.; Kang, Y.; Zhao, Y.; Wang, L.; Liu, J.; Li, Y.; Liang, Z.; He, X.; Li, X.; Tavajohi, N.; Li, B. A review of lithium-ion battery safety concerns: The issues, strategies, and testing standards. *J. Energy Chem.* **2021**, *59*, 83−99.
(3) Lian, P.-J.; Zhao, B.-S.; Zhang, L.-Q.; Xu, N.; Wu, M.-T.; Gao, X.-P. Inorganic sulfide solid electrolytes for all-solid-state lithium secondary batteries. *J. Mater. Chem. A* **2019**, *7* (36), 20540−20557.
(4) Xu, L.; Tang, S.; Cheng, Y.; Wang, K.; Liang, J.; Liu, C.; Cao, Y.-C.; Wei, F.; Mai, L. Interfaces in Solid-State Lithium Batteries. *Joule* **2018**, *2* (10), 1991−2015.
(5) Kato, Y.; Hori, S.; Saito, T.; Suzuki, K.; Hirayama, M.; Mitsui, A.; Yonemura, M.; Iba, H.; Kanno, R. High-power all-solid-state batteries using sulfide superionic conductors. *Nat. Energy* **2016**, *1* (4), 16030.
(6) Randau, S.; Weber, D. A.; Kötz, O.; Koerver, R.; Braun, P.; Weber, A.; Ivers-Tiffée, E.; Adermann, T.; Kulisch, J.; Zeier, W. G.; et al. Benchmarking the performance of all-solid-state lithium batteries. *Nat. Energy* **2020**, *5* (3), 259−270.
(7) Fang, R.; Xu, H.; Xu, B.; Li, X.; Li, Y.; Goodenough, J. B. Reaction Mechanism Optimization of Solid-State Li-S Batteries with a PEO-Based Electrolyte. *Adv. Funct. Mater.* **2021**, *31* (2), 2001812.
(8) Fang, R.; Liu, Y.; Li, Y.; Manthiram, A.; Goodenough, J. B. Achieving stable all-solid-state lithium-metal batteries by tuning the cathode-electrolyte interface and ionic/electronic transport within the cathode. *Mater. Today* **2023**, *64*, 52−60.
(9) Liu, Y.-N.; Xiao, Z.; Zhang, W.-K.; Zhang, J.; Huang, H.; Gan, Y.-P.; He, X.-P.; Kumar, G. G.; Xia, Y. Poly(m-phenylene isophthalamide)-reinforced polyethylene oxide composite electrolyte with high mechanical strength and thermostability for all-solid-state lithium metal batteries. *Rare Met.* **2022**, *41* (11), 3762−3773.
(10) Xia, Y.; Wang, Q.; Liu, Y.; Zhang, J.; Xia, X.; Huang, H.; Gan, Y.; He, X.; Xiao, Z.; Zhang, W. Three-dimensional polyimide nanofiber framework reinforced polymer electrolyte for all-solid-state lithium metal battery. *J. Colloid Interface Sci.* **2023**, *638*, 908−917.
(11) Fang, R.; Li, Y.; Wu, N.; Xu, B.; Liu, Y.; Manthiram, A.; Goodenough, J. B. Ultra-Thin Single-Particle-Layer Sodium Beta-Alumina-Based Composite Polymer Electrolyte Membrane for Sodium-Metal Batteries. *Adv. Funct. Mater.* **2023**, *33* (6), 2211229.
(12) MacFarlane, D. R.; Forsyth, M. Plastic Crystal Electrolyte Materials: New Perspectives on Solid State Ionics. *Adv. Mater.* **2001**, *13* (12−13), 957−966.
(13) Pringle, J. M.; Howlett, P. C.; MacFarlane, D. R.; Forsyth, M. Organic ionic plastic crystals: recent advances. *J. Mater. Chem.* **2010**, *20* (11), 2056−2062.
(14) Pringle, J. M. Recent progress in the development and use of organic ionic plastic crystal electrolytes. *Phys. Chem. Chem. Phys.* **2013**, *15* (5), 1339−1351.
(15) Thomas, M. L.; Hatakeyama-Sato, K.; Nanbu, S.; Yoshizawa-Fujita, M. Organic ionic plastic crystals: flexible solid electrolytes for lithium secondary batteries. *Energy Adv.* **2023**, *2* (6), 748−764.
(16) Zhu, H.; MacFarlane, D. R.; Pringle, J. M.; Forsyth, M. Organic Ionic Plastic Crystals as Solid-State Electrolytes. *Trends Chem.* **2019**, *1* (1), 126−140.
(17) Yunis, R.; Newbegin, T. W.; Hollenkamp, A. F.; Pringle, J. M. Ionic liquids and plastic crystals with a symmetrical pyrrolidinium cation. *Mater. Chem. Front.* **2018**, *2* (6), 1207−1214.
(18) Yoshizawa-Fujita, M.; Yamada, H.; Yamaguchi, S.; Zhu, H.; Forsyth, M.; Takeoka, Y.; Rikukawa, M. Synthesis and Characteristics of Pyrrolidinium-Based Organic Ionic Plastic Crystals with Various Sulfonylamide Anions. *Batteries Supercaps* **2020**, *3* (9), 884−891.
(19) Yamada, H.; Miyachi, Y.; Takeoka, Y.; Rikukawa, M.; Yoshizawa-Fujita, M. Pyrrolidinium-based organic ionic plastic crystals: Relationship between side chain length and properties. *Electrochim. Acta* **2019**, *303*, 293−298.
(20) MacFarlane, D. R.; Huang, J.; Forsyth, M. Lithium-doped plastic crystal electrolytes exhibiting fast ion conduction for secondary batteries. *Nature* **1999**, *402* (6763), 792−794.
(21) Howlett, P. C.; Ponzio, F.; Fang, J.; Lin, T.; Jin, L.; Iranipour, N.; Efthimiadis, J. Thin and flexible solid-state organic ionic plastic crystal-polymer nanofibre composite electrolytes for device applications. *Phys. Chem. Chem. Phys.* **2013**, *15* (33), 13784−13789.
(22) Zhou, Y.; Wang, X.; Zhu, H.; Yoshizawa-Fujita, M.; Miyachi, Y.; Armand, M.; Forsyth, M.; Greene, G. W.; Pringle, J. M.; Howlett, P. C. Solid-State Lithium Conductors for Lithium Metal Batteries Based on Electrospun Nanofiber/ Plastic Crystal Composites. *ChemSusChem* **2017**, *10* (15), 3135−3145.
(23) Wang, X.; Zhu, H.; Greene, G. W.; Zhou, Y.; Yoshizawa-Fujita, M.; Miyachi, Y.; Armand, M.; Forsyth, M.; Pringle, J. M.; Howlett, P. C. Organic Ionic Plastic Crystal-Based Composite Electrolyte with Surface Enhanced Ion Transport and Its Use in All-Solid-State Lithium Batteries. *Adv. Mater. Technol.* **2017**, *2* (7), 1700046.
(24) Nti, F.; Greene, G. W.; Zhu, H.; Howlett, P. C.; Forsyth, M.; Wang, X. Anion effects on the properties of OIPC/PVDF composites. *Mater. Adv.* **2021**, *2* (5), 1683−1694.
(25) Wang, W.; Fang, Z.; Zhao, M.; Peng, Y.; Zhang, J.; Guan, S. Solid polymer electrolytes based on the composite of PEO-LiFSI and organic ionic plastic crystal. *Chem. Phys. Lett.* **2020**, *747*, 137335.
(26) Adebahr, J.; Ciccosillo, N.; Shekibi, Y.; MacFarlane, D. R.; Hill, A. J.; Forsyth, M. The "filler-effect" in organic ionic plastic crystals: Enhanced conductivity by the addition of nano-sized TiO2. *Solid State Ionics* **2006**, *177* (9−10), 827−831.
(27) Shekibi, Y.; Pas, S. J.; Rocher, N. M.; Clare, B. R.; Hill, A. J.; MacFarlane, D. R.; Forsyth, M. Surprising effect of nanoparticle inclusion on ion conductivity in a lithium doped organic ionic plastic crystal. *J. Mater. Chem.* **2009**, *19* (11), 1635.
(28) Shekibi, Y.; Gray-Weale, A.; MacFarlane, D. R.; Hill, A. J.; Forsyth, M. Nanoparticle Enhanced Conductivity in Organic Ionic Plastic Crystals: Space Charge versus Strain Induced Defect Mechanism. *J. Phys. Chem. C* **2007**, *111* (30), 11463−11468.
(29) Shekibi, Y.; Pringle, J. M.; Sun, J.; Pas, S. J.; Rocher, N. M.; Clare, B. R.; Hill, A. J.; MacFarlane, D. R.; Forsyth, M. Lithium-functionalised silica nanoparticles for enhanced ionic conductivity in an organic ionic plastic crystal. *J. Mater. Chem.* **2010**, *20* (2), 338−344.
(30) Jiang, Z.; Han, Q.; Wang, S.; Wang, H. Reducing the Interfacial Resistance in All-Solid-State Lithium Batteries Based on Oxide Ceramic Electrolytes. *ChemElectroChem* **2019**, *6* (12), 2970−2983.
(31) Huo, H.; Chen, Y.; Li, R.; Zhao, N.; Luo, J.; Pereira da Silva, J. G.; Mücke, R.; Kaghazchi, P.; Guo, X.; Sun, X. Design of a mixed conductive garnet/Li interface for dendrite-free solid lithium metal batteries. *Energy Environ. Sci.* **2020**, *13* (1), 127−134.
(32) Chi, S.-S.; Liu, Y.; Zhao, N.; Guo, X.; Nan, C.-W.; Fan, L.-Z. Solid polymer electrolyte soft interface layer with 3D lithium anode for all-solid-state lithium batteries. *Energy Storage Mater.* **2019**, *17*, 309−316.
(33) Gutiérrez-Pardo, A.; Aguesse, F.; Fernández-Carretero, F.; Siriwardana, A. I.; García-Luis, A.; Llordés, A. Improved Electromechanical Stability of the Li Metal/Garnet Ceramic Interface by a Solvent-Free Deposited OIPC Soft Layer. *ACS Appl. Energy Mater.* **2021**, *4* (3), 2388−2397.
(34) Huang, J.; Hollenkamp, A. F. Thermal Behavior of Ionic Liquids Containing the FSI Anion and the Li+ Cation. *J. Phys. Chem. C* **2010**, *114* (49), 21840−21847.
(35) Reiter, J.; Jeremias, S.; Paillard, E.; Winter, M.; Passerini, S. Fluorosulfonyl-(trifluoromethanesulfonyl)imide ionic liquids with enhanced asymmetry. *Phys. Chem. Chem. Phys.* **2013**, *15* (7), 2565−2571.
(36) Zhou, Z.-B.; Matsumoto, H. Lithium-doped, organic ionic plastic crystal electrolytes exhibiting high ambient-temperature conductivities. *Electrochem. Commun.* **2007**, *9* (5), 1017−1022.

https://doi.org/10.1021/acsomega.4c01137
ACS Omega 2024, 9, 22203−22212

(37) Al-Masri, D.; Yunis, R.; Hollenkamp, A. F.; Pringle, J. M. A symmetrical ionic liquid/Li salt system for rapid ion transport and stable lithium electrochemistry. *Chem. Commun.* **2018**, *54* (29), 3660−3663.
(38) Muenzel, V.; Hollenkamp, A. F.; Bhatt, A. I.; de Hoog, J.; Brazil, M.; Thomas, D. A.; Mareels, I. Comment on "A Comparative Testing Study of Commercial 18650-Format Lithium-Ion Battery Cells" [J. Electrochem. Soc., 162, A1592 (2015)]. *J. Electrochem. Soc.* **2015**, *162* (12), Y11−Y12.
(39) Mier, F. A.; Hill, S. M. M.; Lamb, J.; Hargather, M. J. Non-invasive internal pressure measurement of 18650 format lithium ion batteries during thermal runaway. *J. Energy Storage* **2022**, *51*, 104322.
(40) Aniya, M.; Ikeda, M. A Model for Non-Arrhenius Ionic Conductivity. *Nanomaterials* **2019**, *9*, 911.
(41) Maryati, Y.; Winarsih, S.; Syakuur, M. A.; Manawan, M.; Saragi, T.; Risdiana. Structural Properties and Hopping Conduction in the Normal State of Electron-Doped Superconductor Cuprate $Eu_{2-<i>x</i>}Ce_{<i>x</i>}CuO_{4+\alpha-\delta}$. *ACS Omega* **2022**, *7* (15), 12601−12609.
(42) Henderson, W. A.; Seo, D. M.; Zhou, Q.; Boyle, P. D.; Shin, J.-H.; De Long, H. C.; Trulove, P. C.; Passerini, S. An Alternative Ionic Conductivity Mechanism for Plastic Crystalline Salt-Lithium Salt Electrolyte Mixtures. *Adv. Energy Mater.* **2012**, *2* (11), 1343−1350.
(43) Li, Y.; Han, J.-T.; Wang, C.-A.; Vogel, S. C.; Xie, H.; Xu, M.; Goodenough, J. B. Ionic distribution and conductivity in lithium garnet Li7La3Zr2O12. *J. Power Sources* **2012**, *209*, 278−281.
(44) Nti, F.; Porcarelli, L.; Greene, G. W.; Zhu, H.; Makhlooghiazad, F.; Mecerreyes, D.; Howlett, P. C.; Forsyth, M.; Wang, X. The influence of interfacial interactions on the conductivity and phase behaviour of organic ionic plastic crystal/polymer nanoparticle composite electrolytes. *J. Mater. Chem. A* **2020**, *8* (10), 5350−5362.
(45) Maier, J. Ionic conduction in space charge regions. *Prog. Solid State Chem.* **1995**, *23* (3), 171−263.
(46) Nomura, Y.; Yamamoto, K.; Hirayama, T.; Ouchi, S.; Igaki, E.; Saitoh, K. Direct Observation of a Li-Ionic Space-Charge Layer Formed at an Electrode/Solid-Electrolyte Interface. *Angew. Chem., Int. Ed.* **2019**, *58* (16), 5292−5296.
(47) Lee, H.; Yang, S.; Kim, S.; Song, J.; Park, J.; Doh, C.-H.; Ha, Y.-C.; Kwon, T.-S.; Lee, Y. M. Understanding the effects of diffusion coefficient and exchange current density on the electrochemical model of lithium-ion batteries. *Curr. Opin. Electrochem.* **2022**, *34*, 100986.
(48) Howlett, P. C.; Shekibi, Y.; MacFarlane, D. R.; Forsyth, M. Li-Metal Symmetrical Cell Studies Using Ionic Organic Plastic Crystal Electrolyte. *Adv. Eng. Mater.* **2009**, *11* (12), 1044−1048.
(49) Howlett, P. C.; Sunarso, J.; Shekibi, Y.; Wasser, E.; Jin, L.; MacFarlane, D. R.; Forsyth, M. On the use of organic ionic plastic crystals in all solid-state lithium metal batteries. *Solid State Ionics* **2011**, *204−205*, 73−79.
(50) Jin, L.; Howlett, P.; Efthimiadis, J.; Kar, M.; Macfarlane, D.; Forsyth, M. Lithium doped N,N-dimethyl pyrrolidinium tetrafluoroborate organic ionic plastic crystal electrolytes for solid state lithium batteries. *J. Mater. Chem.* **2011**, *21* (27), 10171−10178.

https://doi.org/10.1021/acsomega.4c01137
ACS Omega 2024, 9, 22203−22212